Epitaxial Growth and Air-Stability of Monolayer Antimonene on PdTe$_2$

Xu Wu, Yan Shao, Hang Liu, Zili Feng, Ye-Liang Wang,* Jia-Tao Sun, Chen Liu, Jia-Ou Wang, Zhong-Liu Liu, Shi-Yu Zhu, Yu-Qi Wang, Shi-Xuan Du, You-Guo Shi, Kurash Ibrahim, and Hong-Jun Gao*

Investigation of 2D materials has developed rapidly in recent years,[1,2] inspired by their unique properties and the promise of many valuable applications. In addition to graphene, researchers have developed novel 2D materials with delicate properties suitable for a wide range of innovative applications. Several single atomic-layer materials with graphene-like honeycombs, such as silicene[3–6] (made up of silicon), germanene[7–9] (germanium), hafnene[10] (hafnium), stanene[11] (tin), and blue phosphorus,[12] holding exotic properties for next-generation information nanodevices, were successfully fabricated by epitaxy. These monoelemental materials have a gap over gapless graphene, giving them an important advantage for application in nanoelectronic devices. Still, the gap in these 2D materials is small, limiting their application in electronics. It is imperative to obtain 2D materials with more useful bandgaps. Recently, many theoretical papers have reported a novel graphene-like 2D honeycomb lattice of antimony atoms, called "antimonene."[13–19] A bandgap of 2.28 eV is predicted[13] for monolayer antimonene. Such a wide bandgap larger than 2.0 eV would make antimonene very intriguing for applications in metal-oxide-semiconductor field-effect-transistors (MOSFETs)[18] and, especially, photoelectric devices,[19] as theoretically predicted. In addition to the wide bandgap, monolayer antimonene is predicted to be a topological insulator,[15] making it possible for high-efficiency quantum transport and topological quantum computation.[20,21] Thus, to confirm these theoretical descriptions of antimonene experimentally,

finding an effective method for fabrication of an antimonene monolayer is of great importance. Very recently, mechanical isolation of few-layer antimonene flakes from antimony bulk was reported.[22] Nevertheless, to the best of our knowledge, epitaxial growth of monolayer antimonene has not yet been realized.

Here, we report the growth of monolayer antimonene on a 2D layered PdTe$_2$ substrate by molecular beam epitaxy (MBE). We chose PdTe$_2$ as the substrate for at least two reasons. First, its crystal periodicity (the surface lattice constant is 4.10 Å) has a very small mismatch (less than 2.3%) with that of free-standing antimonene (the calculated lattice constant of which is 4.01 Å).[23,24] Second, it has a chemically stable surface, typical of a layered transition-metal-dichalcogenide (TMD) material.[25] The antimony atoms were first deposited onto a PdTe$_2$ surface kept at a proper temperature, whereupon a distinct well-ordered structure was observed by in situ low-energy electron diffraction (LEED). The atomic structure of this monolayer antimonene was determined by scanning tunneling microscopy (STM). Then we performed first-principles calculations based on density functional theory (DFT) to elucidate the experimental results. Combining our experimental observations and the theoretic calculations, we verified that the antimonene fabricated on a PdTe$_2$ substrate is a 2D continuous monolayer with a buckled conformation. Moreover, our findings reveal that the antimonene layer interacts only weakly with the PdTe$_2$ substrate and, more important, is quite inert with respect to the air. This high-quality epitaxial antimonene with a large bandgap and chemical stability is promising for applications in nanoelectronic devices.

Figure 1 shows the monolayer antimonene film fabricated through epitaxial growth of antimony atoms on the PdTe$_2$ surface. The PdTe$_2$ substrate was cleaved in situ from a bulk single crystal sample and then was checked by STM (see Figure S1, Supporting Information) in order to obtain well-ordered large-scale monolayer antimonene film, the PdTe$_2$ substrate was kept at 400 K while depositing Sb atoms onto it (as shown by a schematic in Figure 1a). An atomically smooth film was obtained under these experimental conditions, as shown in Figure 1b. The ordering and symmetry of this film was characterized macroscopically by LEED, as shown in the inset in Figure 1b. Only six diffraction spots exist in this LEED pattern, representing an almost commensurate (1 × 1) lattice with respect to the PdTe$_2$ surface. These diffraction spots originate from the lattice of both the antimonene film and the PdTe$_2$ substrate, since they have quite similar lattice constants. The clear and simple LEED

X. Wu, Y. Shao, H. Liu, Z. Feng, Prof. Y.-L. Wang,
Dr. J.-T. Sun, Z.-L. Liu, S.-Y. Zhu, Y.-Q. Wang,
Prof. S.-X. Du, Prof. Y.-G. Shi, Prof. H.-J. Gao
Institute of Physics and University of Chinese
Academy of Sciences
Chinese Academy of Sciences
Beijing 100190, China
E-mail: ylwang@iphy.ac.cn; hjgao@iphy.ac.cn
Prof. Y.-L. Wang, Prof. S.-X. Du, Prof. H.-J. Gao
Collaborative Innovation Center of Quantum Matter
Beijing 100084, China
Prof. Y.-L. Wang, Prof. S.-X. Du, Prof. H.-J. Gao
Beijing Key Laboratory for Nanomaterials and Nanodevices
Beijing 100190, China
C. Liu, Dr. J.-O. Wang, Prof. K. Ibrahim
Institute of High Energy Physics
Chinese Academy of Sciences
Beijing 100049, China

COMMUNICATION
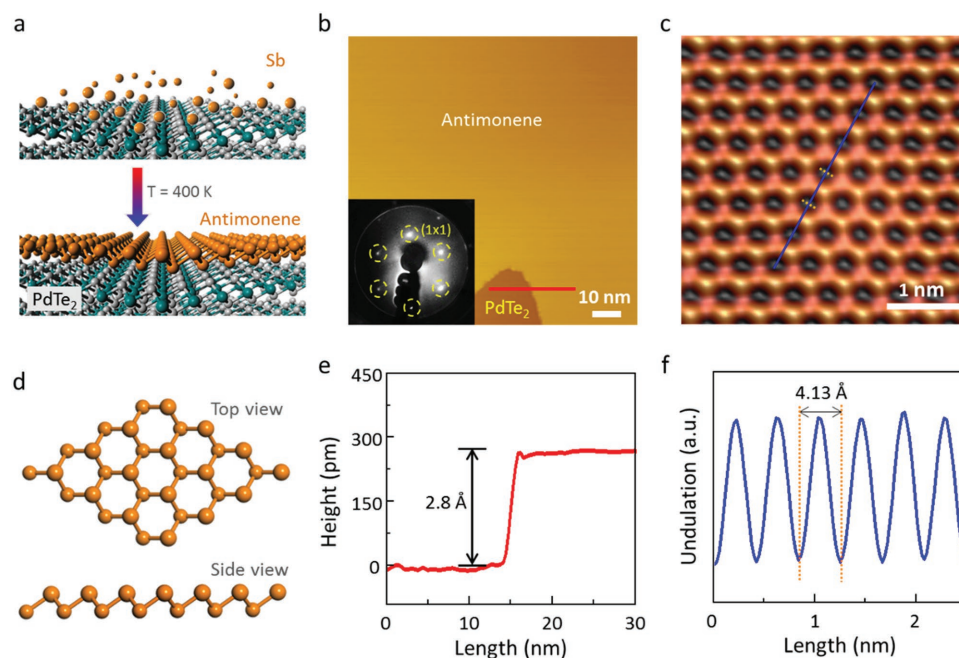
Figure 1. Monolayer antimonene formed on PdTe$_2$ substrate. a) Schematic of fabrication. b) STM topographic image (−2.0 V, −10 pA) of large antimonene island on PdTe$_2$. Inset: LEED pattern of antimonene on PdTe$_2$. The six diffraction spots are due to the antimonene (1 × 1) structure with respect to the substrate. c) Atomic resolution STM image (−1.5 V, −200 pA) of monolayer antimonene with enhanced visibility showing the graphene-like honeycomb. d) Top view (upper) and side view (lower) of the buckled conformation of the antimonene honeycomb. e) A height profile along the red line in (b), showing that the apparent height of the antimonene island is 2.8 Å. f) Line profile corresponding to the blue line in (c), revealing the periodicity of the antimonene lattice (4.13 ± 0.02 Å).

pattern in reciprocal space thus suggests the formation of an antimony adlayer that is a well-ordered and single-crystalline network with a periodicity similar to that of the PdTe$_2$ substrate. The formation of the high-quality antimony adlayer was further confirmed by atomic-resolved STM observations in real space as described below.
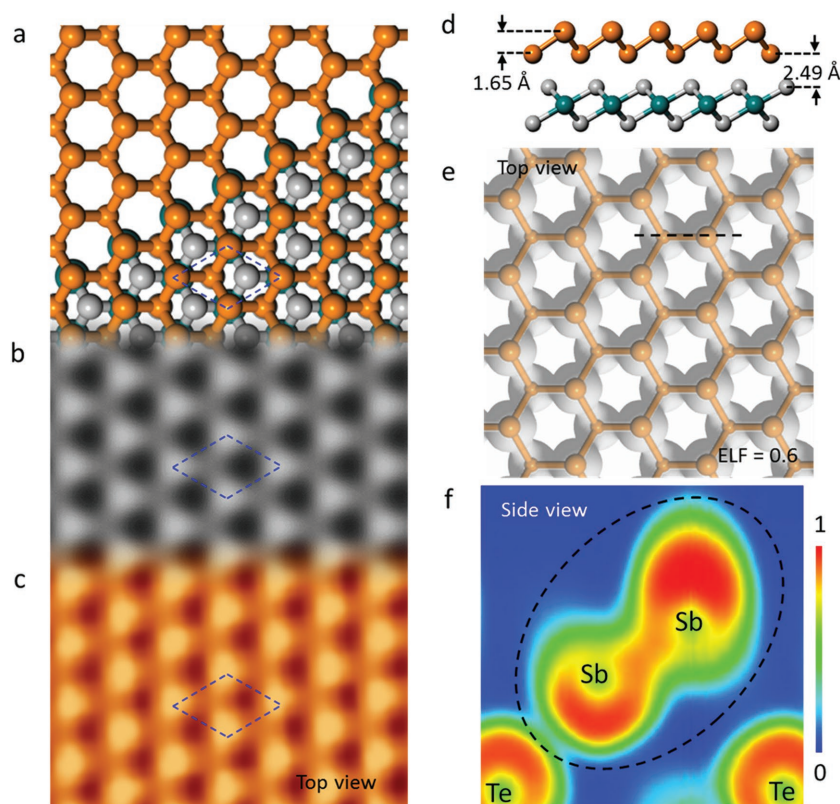
In order to gain a fuller understanding of this antimony film in detail, the STM measurements were carried out. Figure 1b shows a typical STM image in large scale, revealing an antimonene adlayer on the PdTe$_2$ surface with a large area and high quality. This film is smooth and uniform with no obvious defects or domain boundaries in it. The apparent height of this antimonene adlayer is ≈2.8 Å (Figure 1e), as measured by the profile line across the edge of the antimonene film (corresponding to the red line in Figure 1b). This height is close to that of a single layer of antimonene in the Sb bulk, which is calculated to be 3.38 Å.[13] So these measurements indicate that the antimony adlayer is a monolayer.

A high-resolution STM image of monolayer antimonene is displayed in Figure 1c, in which the graphene-like honeycomb lattice can be clearly seen. Specifically, from our atom-resolved STM measurements, a buckled configuration of this honeycomb lattice can be well distinguished, as illustrated by the schematic in Figure 1d. This corrugation in antimonene is in agreement with the previous work wherein antimonene is theoretically predicted to be a 2D structure with a buckled honeycomb lattice consisting of two sublattices in different atomic layers.[13] Furthermore, to reveal the lattice periodicity of this monolayer antimonene clearly, we obtained the height profile

(Figure 1f) of the buckled honeycomb lattice along the blue line in Figure 1c. It indicates a periodicity of 4.13 ± 0.02 Å in the graphene-like honeycomb lattice. This value is quite close to the periodicity of the PdTe$_2$ substrate (4.10 ± 0.02 Å, see Figure S1c, Supporting Information) with a small difference of less than 0.5%, as measured in our experiment. So the close match of these lattices, seen from STM observations, is consistent with the LEED pattern showing (1 × 1) diffraction points. By these experimental data, we for the first time unveil the morphology and configuration of epitaxial monolayer antimonene at atomic scale.

To further elucidate the experimental results above, we carried out first-principles theoretic calculations. Three different models of antimonene on PdTe$_2$ were considered by taking the lowest Sb atom in the bulk antimonene as the location reference on the substrate lattice—that is, the lower Sb atom was located on three different positions on the PdTe$_2$ substrate (on the Pd atom, on the lower Te atom, and on the upper Te atom, respectively, as shown in Figure S1, Supporting Information). All these three models are fully relaxed, and the most stable structure with the lowest binding energy is obtained. In this most stable structure, the lowest Sb atom is located on top of the lower Te atom (see **Figure 2**a and Figure S2b, Supporting Information).

According to the optimized model, a simulated STM image was obtained (Figure 2b). The overall features in simulations are remarkably consistent with the STM observations, as shown in Figure 2c by an atomic-resolution STM image of antimonene on PdTe$_2$ obtained at a sample bias voltage. In detail,

ADVANCED
SCIENCE NEWS
www.advancedsciencenews.com

**ADVANCED
MATERIALS**
www.advmat.de

COMMUNICATION

Figure 2. DFT calculations and atomic configuration of monolayer antimonene on a PdTe$_2$ substrate. a) Top view of the relaxed model that has the lowest binding energy of the antimonene with the PdTe$_2$ substrate. Orange, gray, and cyan balls represent Sb, Te, and Pd atoms, respectively. For clarity, some of the substrate atoms are omitted. b) Simulated STM image, showing features remarkably consistent with the experimental results in the same triangular sublattice. The dashed line rhombus denotes two triangular sublattices of one unit cell in the antimonene. c) Atomic resolution STM image (−2.0 V, −300 pA) of the antimonene layer. d) Side view of the relaxed structure of antimonene on PdTe$_2$. The distance between the top and bottom Sb sublayers is 1.65 Å, and the distance between the bottom Sb plane and the top Te plane of PdTe$_2$ is 2.49 Å. d) Top view of the overall ELF of the relaxed model with an ELF value of 0.6, showing the continuity of the monolayer antimonene. f) ELF of the cross section along the black dotted line in (e), demonstrating high localization of the electrons in Sb—Sb pairs.

in the STM image of this graphene-like monolayer antimonene on PdTe$_2$, the upper Sb atoms are brighter and the lower Sb atoms are dimmer. This causes a distinct contrast between two triangular regions in a unit cell, as marked by a dashed-line rhombus.

Specifically, the calculated surface crystalline constant in the most stable model is 4.12 Å, which is consistent with the value from STM observations (Figure 1f). The side view of the calculated model is shown in Figure 2d. It indicates the undulation between two Sb sublayers is 1.65 Å, almost equal to the undulation in the bulk Sb material. The distance between the Sb layer and the substrate is 2.49 Å, which is significantly larger than the distance among antimonene layers in bulk Sb. This larger layer-by-layer distance suggests a weak interaction between the epitaxial antimonene film and the substrate.

To gauge the interfacial interaction of the antimonene network on the PdTe$_2$ substrate further, the electron localization function (ELF)[26,27] was calculated. ELF allows one to evaluate chemical interactions directly from the charge localization

between individual atoms. The value of ELF is in the range from 0 to 1, meaning that the electrons' localization ranges from zero to high localization. Here, a calculated isosurface with an ELF value of 0.6 for the most stable structure is shown in Figure 2e. We can see that the electrons of monolayer antimonene are localized around the Sb atoms and the region between the nearest Sb atoms. Figure 2e thus intuitively illustrates the formation of a continuous antimonene layer.

A cross-section ELF pattern perpendicular to the plane of the monolayer antimonene and along the Sb—Sb bonding direction (corresponding to the black dotted line in Figure 2e) is shown in Figure 2f. It is clear that electrons are highly localized at the Sb–Sb pair with an ELF value larger than 0.8. This provides direct evidence of a strong chemical interaction between each Sb—Sb pair, responsible for the existence and stability of the structure of antimonene. Moreover, in the optimized model in Figure 2f, the distance between the lower Sb atom in antimonene and the upper layer Te atom in the substrate is the shortest one, and this is the region with the strongest coupling between the antimonene and the substrate. Even for this strongest coupling region, the ELF value is still less than 0.3, which is somewhat smaller than the ELF value of Sb—Sb pairs. Thus, this vanishing ELF at the interface indicates a kind of van der Waals interfacial interaction between the Sb monolayer and the PdTe$_2$ substrate. In short, this quantitative analysis demonstrates that a strong binding energy exists within the Sb monolayer and a weak interaction exists at the interface. With all this evidence combined, we can conclude that a continuous 2D antimonene monolayer has been successfully fabricated on the PdTe$_2$ substrate.

To further analyze the interaction between the monolayer antimonene and the substrate experimentally, we obtained X-ray photoelectron spectroscopy (XPS) measurements of the sample before and after formation of the monolayer antimonene. **Figure 3**a,b shows characteristic XPS spectra from the core level of the Pd and Te. As shown in Figure 3a, for the bare substrate, the characteristic signals of Pd $3d_{3/2}$ and $3d_{5/2}$ appear as peaks at their binding energies of 341.9 and 336.6 eV, respectively. After antimonene is deposited, the binding energy positions of these two representative peaks remain unchanged, and the shape of the curve is the same as before. Moreover, for the XPS core level spectrum of Te, as shown in Figure 3b, there is also no obvious change in the binding energies of the characteristic peaks and the shapes of the peaks. Figure 3c presents the XPS core-level spectrum of Sb 4d from the antimonene adlayer. The Sb $4d_{5/2}$ spectrum

COMMUNICATION
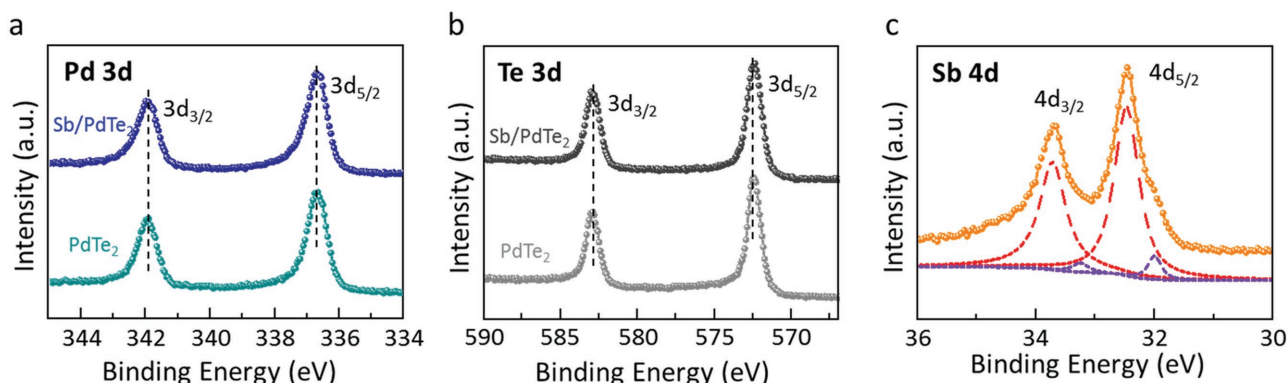
Figure 3. XPS results of the antimonene monolayer on the PdTe₂ substrate. a) The Pd 3d core level spectra before (lower) and after (upper) formation of the antimonene monolayer. The peak positions (at binding energy of 341.9 and 336.6 eV) and shapes have not changed during formation of the antimonene. b) The Te 3d spectra. Similarly, the peak positions (582.9 and 572.5 eV) and shapes have not changed during antimonene formation. c) Sb 4d core level spectrum. The dominant red peaks (33.60 and 32.35 eV) can be assigned to the Sb in antimonene. The tiny purple peaks (33.30 and 32.05 eV) can be assigned to Sb atoms not yet formed into antimonene.

appears as two peaks, at 32.35 and 32.05 eV. The violet peak represents the small Sb clusters on the substrate. The red peak at 32.35 eV, which is the dominant part of the Sb $4d_{5/2}$ peak, has binding energy close to that of bulk Sb ($\approx$31.9–32.3 eV).[28]

Since the change in the chemical state of the element is easy to detect by XPS, our XPS measurements indicate that there is no obvious difference of chemical state of the Pd and Te in the substrate before and after formation of the antimonene adlayer. These XPS measurements further verify that there is no chemical interfacial coupling between the antimonene and the PdTe₂ substrate, which is consistent with the calculated ELF mentioned above. In short, the substrate has no obvious effect on the electronic structure of the epitaxial monolayer antimonene.

Chemical stability is a critical property for a material in electronic applications, especially for atomic-thickness 2D materials. To investigate the stability of the antimonene monolayer in air, we performed an experiment on the monolayer antimonene sample by venting air into the chamber where the sample was stored. Since the chemical reaction normally starts from the edges of 2D materials, we used a sample with lower Sb coverage, featuring small antimonene islands with plenty of edges. Before being exposed to air, the sample was characterized by STM and XPS as shown in **Figure** 4a,d (orange curve), respectively. The topographic STM image reveals that the antimonene islands are clean and smooth with no obvious impurity on the
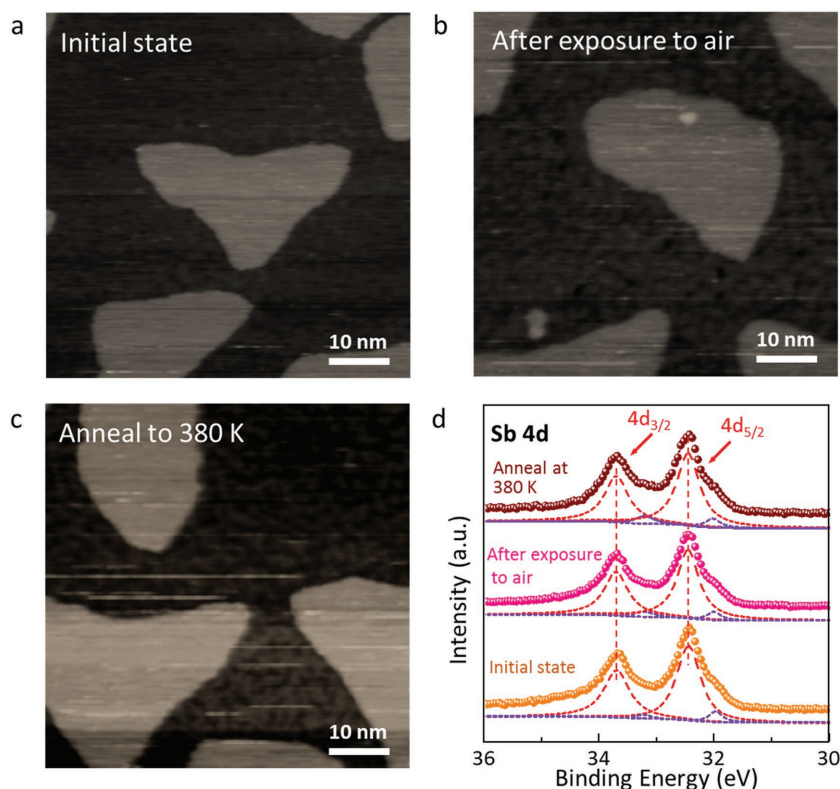
Figure 4. Chemical stability of antimonene islands. a) Typical STM image (−2.0 V, −100 pA) of antimonene islands on PdTe₂ substrate before air exposure. The surface of the islands is smooth without impurities. b) STM image (−2.0 V, −100 pA) of the same sample after exposing to air for 20 min. c) STM image of the same sample after annealing to 380 K. The small spots have disappeared and the surface of the antimonene islands has become clean and smooth again. d) XPS measurements of the same sample. The upper (wine), middle (pink), and lower (orange) curves represent the Sb 4d spectrum before exposure to air, after air exposure, and after annealing to 380 K, respectively. The peaks' positions and shapes in these three curves have not changed, demonstrating that the antimonene is chemically inert to air. The photon energy of XPS experiments in (d) for Sb 4d measurements is 180 eV.

ADVANCED
SCIENCE NEWS
www.advancedsciencenews.com

ADVANCED
MATERIALS
www.advmat.de

COMMUNICATION

islands. Then the sample was exposed to air and kept at room temperature (300 K) for 20 min. The pressure of air was 1×10^5 Pa. After exposing it to air, we kept the sample at room temperature and measured it again with STM and XPS, as shown in Figure 4b,d (pink curve). In the typical STM image in Figure 4b, few bright spots appear at the surface of the antimonene islands, suggesting some adsorbate on the islands. It is very interesting that the curve of the Sb 4d peak in the XPS result in Figure 4d is unchanged after air exposure, meaning that no chemical reaction of the antimony happened during air exposure. Moreover, we annealed the sample at 380 K for 10 min to de-gas it. Figure 4c,d (wine curve) shows a typical STM image and the XPS result after annealing. It is interesting that the STM image is quite similar to the result before air exposure. The XPS curve is also consistent with the one before the exposure. These combined measurements are strong evidence that the Sb atoms of monolayer antimonene are quite inert to air. Very chemically inert, wide-bandgap antimonene obviously has potential for future electronic applications.

In summary, we have successfully grown monolayer antimonene on a PdTe$_2$ substrate. LEED and STM measurements demonstrate high quality of the epitaxial antimonene. Such monolayer antimonene has a buckled graphene-like configuration. In addition, calculations reveal that the Sb atoms chemically bind directly to each other. The interaction between monolayer antimonene and the substrate is via a weak van der Waals force, as demonstrated by experimental XPS measurements. Moreover, STM and XPS measurements from our air exposure experiment show the excellent stability of monolayer antimonene. This work provides an effective method to produce high-quality monolayer antimonene that is very chemically inert and has a large bandgap, a significant advance for developing electronic and optoelectronic nanodevices.

Experimental Section

Sample Preparation and STM Experiments: The antimonene monolayer was fabricated on a PdTe$_2$ substrate in an ultrahigh vacuum (UHV) chamber, with a base pressure of 2×10^{-10} mbar, equipped with standard MBE capabilities. The PdTe$_2$ substrate was cleaved from the single crystal in UHV. Antimony atoms (Sigma, 99.999%) evaporated from a Knudsen cell were deposited onto the freshly cleaved PdTe$_2$ substrate, kept at 400 K. After growth, the sample was transferred to a chamber with LEED and STM equipment for measurements. In the oxidation experiment, the sample was exposed to pure air at a pressure of 1×10^5 Pa for 20 min in a load-lock chamber, and then was transferred back into the UHV chamber to further obtain STM or XPS measurements. All STM measurements were performed at room temperature with a chemical etched W tip.

XPS Measurements: The in situ X-ray photoelectron spectroscopy measurements were performed at the Beijing Synchrotron Radiation Facility (BSRF). The samples were stored in a UHV suitcase for transfer among different experimental stations. The synchrotron radiation light monochromated by four high-resolution gratings and controlled by a hemispherical energy analyzer has a photon energy in the range from 10 to 1100 eV. The photon energy of XPS experiments was 500 eV for Pd 3d, 720 eV for Te 3d, and 180 eV for Sb 4d measurements, respectively.

Calculation Method: The density-functional calculations were performed with the Vienna ab initio simulation package (VASP)[29] using projector-augmented wave (PAW) pseudopotential in conjunction with the Perdew–Burke–Ernzerhof (PBE) functional, and the plane-wave basis was set to an energy cutoff of 500 eV. The calculation model consisted of monolayer Sb, monolayer PdTe$_2$, and a vacuum layer larger than 20 Å. All the structures were relaxed until the force on each atom was less than 0.01 eV Å^{-1} and the break condition for the electronic self-consistent loop was 1×10^{-5} eV. The Brillouin zone was sampled by a $(12 \times 12 \times 1)$ Gamma centered k-mesh.

Supporting Information

Supporting Information is available from the Wiley Online Library or from the author.

Acknowledgements

[1] A. K. Geim, I. V. Grigorieva, *Nature* **2013**, *499*, 419.
[2] A. H. C. Neto, F. Guinea, N. M. R. Peres, K. S. Novoselov, A. K. Geim, *Rev. Mod. Phys.* **2009**, *81*, 109.
[3] B. Feng, Z. Ding, S. Meng, Y. Yao, X. He, P. Cheng, L. Chen, K. Wu, *Nano Lett.* **2012**, *12*, 3507.
[4] A. Fleurence, R. Friedlein, T. Ozaki, H. Kawai, Y. Wang, Y. Yamada-Takamura, *Phys. Rev. Lett.* **2012**, *108*, 245501.
[5] L. Meng, Y. Wang, L. Zhang, S. Du, R. Wu, L. Li, Y. Zhang, G. Li, H. Zhou, W. A. Hofer, H. J. Gao, *Nano Lett.* **2013**, *13*, 685.
[6] D. Chiappe, E. Scalise, E. Cinquanta, C. Grazianetti, B. van den Broek, M. Fanciulli, M. Houssa, A. Molle, *Adv. Mater.* **2014**, *26*, 2096.
[7] M. Derivaz, D. Dentel, R. Stephan, M. C. Hanf, A. Mehdaoui, P. Sonnet, C. Pirri, *Nano Lett.* **2015**, *15*, 2510.
[8] L. Li, S. Z. Lu, J. Pan, Z. Qin, Y. Q. Wang, Y. Wang, G. Y. Cao, S. Du, H. J. Gao, *Adv. Mater.* **2014**, *26*, 4820.
[9] L. Zhang, P. Bampoulis, A. N. Rudenko, Q. Yao, A. van Houselt, B. Poelsema, M. I. Katsnelson, H. J. Zandvliet, *Phys. Rev. Lett.* **2016**, *116*, 256804.
[10] L. Li, Y. Wang, S. Xie, X. B. Li, Y. Q. Wang, R. Wu, H. Sun, S. Zhang, H. J. Gao, *Nano Lett.* **2013**, *13*, 4671.
[11] F. F. Zhu, W. J. Chen, Y. Xu, C. L. Gao, D. D. Guan, C. H. Liu, D. Qian, S. C. Zhang, J. F. Jia, *Nat. Mater.* **2015**, *14*, 1020.
[12] J. L. Zhang, S. Zhao, C. Han, Z. Wang, S. Zhong, S. Sun, R. Guo, X. Zhou, C. D. Gu, K. D. Yuan, Z. Li, W. Chen, *Nano Lett.* **2016**, *16*, 4903.
[13] S. Zhang, Z. Yan, Y. Li, Z. Chen, H. Zeng, *Angew. Chem., Int. Ed.* **2015**, *54*, 3112.
[14] P. F. Zhang, Z. Liu, W. H. Duan, F. Liu, J. Wu, *Phys. Rev. B* **2012**, *85*, 201410.
[15] F. C. Chuang, C. H. Hsu, C. Y. Chen, Z. Q. Huang, V. Ozolins, H. Lin, A. Bansil, *Appl. Phys. Lett.* **2013**, *102*, 022424.

COMMUNICATION

[16] G. Bian, X. Wang, Y. Liu, T. Miller, T. C. Chiang, *Phys. Rev. Lett.* **2012**, *108*, 176401.

[17] G. Bian, T. Miller, T. C. Chiang, *Phys. Rev. Lett.* **2011**, *107*, 036802.

[18] G. Pizzi, M. Gibertini, E. Dib, N. Marzari, G. Iannaccone, G. Fiori, *Nat. Commun.* **2016**, *7*, 12585.

[19] X. P. Chen, Q. Yang, R. S. Meng, J. K. Jiang, Q. H. Liang, C. J. Tan, X. Sun, *J. Mater. Chem. C* **2016**, *4*, 5434.

[20] M. X. Wang, C. Liu, J. P. Xu, F. Yang, L. Miao, M. Y. Yao, C. L. Gao, C. Shen, X. Ma, X. Chen, Z. A. Xu, Y. Liu, S. C. Zhang, D. Qian, J. F. Jia, Q. K. Xue, *Science* **2012**, *336*, 52.

[21] Y. Q. Wang, X. Wu, Y. L. Wang, Y. Shao, T. Lei, J. O. Wang, S. Y. Zhu, H. Guo, L. X. Zhao, G. F. Chen, S. Nie, H. M. Weng, K. Ibrahim, X. Dai, Z. Fang, H. J. Gao, *Adv. Mater.* **2016**, *28*, 5013.

[22] P. Ares, F. Aguilar-Galindo, D. Rodríguez-San-Miguel, D. A. Aldave, S. Díaz-Tendero, M. Alcamí, F. Martín, J. Gómez-Herrero, F. Zamora, *Adv. Mater.* **2016**, *28*, 6332.

[23] T. R. Finlayson, W. Reichardt, H. G. Smith, *Phys. Rev. B* **1986**, *33*, 2473.

[24] G. W. Ryan, W. L. Sheils, *Phys. Rev. B* **2000**, *61*, 8526.

[25] M. Chhowalla, H. S. Shin, G. Eda, L. J. Li, K. P. Loh, H. Zhang, *Nat. Chem.* **2013**, *5*, 263.

[26] A. D. Becke, K. E. Edgecombe, *J. Chem. Phys.* **1990**, *92*, 5397.

[27] A. Savin, O. Jepsen, J. Flad, O. K. Andersen, H. Preuss, H. G. Vonschnering, *Angew. Chem., Int. Ed.* **1992**, *31*, 187.

[28] P. M. T. M. van Attekum, J. M. Trooster, *Phys. Rev. B* **1979**, *20*, 2335.

[29] D. Vanderbilt, *Phys. Rev. B* **1990**, *41*, 7892.